Chinese Journal of
POLYMER SCIENCE

RESEARCH ARTICLE

https://doi.org/10.1007/s10118-023-2921-7
Chinese J. Polym. Sci. **2023**, *41*, 1223–1229

A Novel CA4P Polymeric Nanoparticle for Murine Hepatoma Therapy

Zhi-Lin Liu[a,b], Xi-Tong Ren[a,b,c], Yue Huang[a,b], Jia-Li Sun[a,b,c], Xiao-Shuang Wang[d], Meng-Fei Zheng[a,b,c], Lin-Jie Cui[a,b,c], Xue-Fei Zhang[e*], and Zhao-Hui Tang[a,b,c*]

[a] *Key Laboratory of Polymer Ecomaterials, Changchun Institute of Applied Chemistry, Chinese Academy of Sciences, Changchun 130022, China*
[b] *Jilin Biomedical Polymers Engineering Laboratory, Changchun 130022, China*
[c] *School of Applied Chemistry and Engineering, University of Science and Technology of China, Hefei 230026, China*
[d] *No. 1 Department of Neurology, China-Japan Union Hospital of Jilin University, Changchun 130033, China*
[e] *Key Laboratory of Environmentally Friendly Chemistry and Applications of Ministry of Education and Key Laboratory of Polymeric Materials & Application Technology of Hunan Province, College of Chemistry, Xiangtan University, Xiangtan 411105, China*

Electronic Supplementary Information

Abstract Combretastatin A4 phosphate (CA4P) is a potent vascular disrupting agent with good water solubility. However, it is only effective at high doses, which decreases clinical applicability. Herein, we designed stable CA4P polymeric nanoparticles (CA4P NPs) consisting of various cholesterol derivatives, and with a drug loading efficacy of 93%. The nanoparticles released CA4P in a sustained manner and achieved a 72% inhibition rate in the murine H22 liver tumor model, which was about 2.9-fold higher than that of free CA4P (24.6%). Furthermore, the carrier components of CA4P NPs were metabolized to arginine, cholesterol, ethanol and poly(ethylene glycol) *in vivo*; therefore, the CA4P NPs are safe and have significant potential for clinical translation.

Keywords CA4P polymeric nanoparticle; Cholesterol derivatives; Vascular disrupting agent; Phosphate-guanidine coordination; Drug controlled release

Citation: Liu, Z. L.; Ren, X. T.; Huang, Y.; Sun, J. L.; Wang, X. S.; Zheng, M. F.; Cui, L. J.; Zhang, X. F.; Tang, Z. H. A novel CA4P polymeric nanoparticle for murine hepatoma therapy. *Chinese J. Polym. Sci.* **2023**, *41*, 1223–1229.

INTRODUCTION

The tumor vascular system provides oxygen and nutrients to the rapidly proliferating cells and is therefore critical for tumor growth and metastasis.[1–3] Thus, vascular disrupting agents (VDAs) are promising anti-tumor drugs since they can "starve" the tumor and induce necrosis by blocking the supply of oxygen and nutrients.[4–6] Since VDAs inhibit tumor growth through "remote" action rather than direct contact,[7–10] they can overcome the limitations of traditional chemotherapy drugs that must penetrate deep into the tumor to be effective.[11,12]

Combretastatin A4 (CA4) is a potent VDA with broad-spectrum anti-tumor activity[13–15] that inhibits tumor vascular endothelial cells by interfering with the nucleation process of microtubulin.[16-19] A phosphate derivative of CA4 (CA4P) was designed to improve its aqueous solubility.[20] CA4P is reduced to CA4 prodrug in the tumor microenvironment with high levels of alkaline phosphatase content. Although CA4P has been tested in a phase II-III clinical trial in combination with a partial drug regimen,[21] it is effective only at high doses (~100 mg/kg) that can cause severe cardiotoxicity.[22–24] Thus, clinical studies on CA4P have been considerably delayed. We previously found that CA4 loaded into nanocarriers can be delivered selectively to the tumor vessels,[25] which can destruct tumor vascular and cause persistent tumor necrosis, eventually resulting in more effective growth suppression.[26] However, we had synthesized CA4 polymeric nanoparticles by attaching the drug to poly(L-glutamic acid)-graft-poly(ethylene glycol) *via* esterification of carboxyl and phenolic hydroxyl, which may cause systemic toxicity if CA4 is accidentally released in the bloodstream.[27] Given that CA4P is less toxic compared to CA4,[28–30] we surmised that CA4P nanodrugs would be more effective and have a greater potential for clinical translation.

Herein, we designed a novel polymeric nanoparticle delivery system by synthesizing and assembling various cholesterol derivatives into CA4P nanoparticles (CA4P NPs) through the coordination of the phosphate group in CA4P with the guanidine group in guanidine-based cholesterol (AE-Chol) (Fig. 1). Stable CA4P NPs with 93% drug loading efficacy (CA4P NPs-4) were obtained after screening various loading methods and achieved sustained release of CA4P. The CA4P NPs-4 inhibited H22 liver tumor growth in a mouse model by 72%, which was about 2.9-fold higher than that of free CA4P (24.6%), and significantly increased necrosis of tumor cells.

* Corresponding authors, E-mail: zxf7515@xtu.edu.cn (X.F.Z.)
E-mail: ztang@ciac.ac.cn (Z.H.T.)

Received November 19, 2022; Accepted December 6, 2022; Published online February 10, 2023

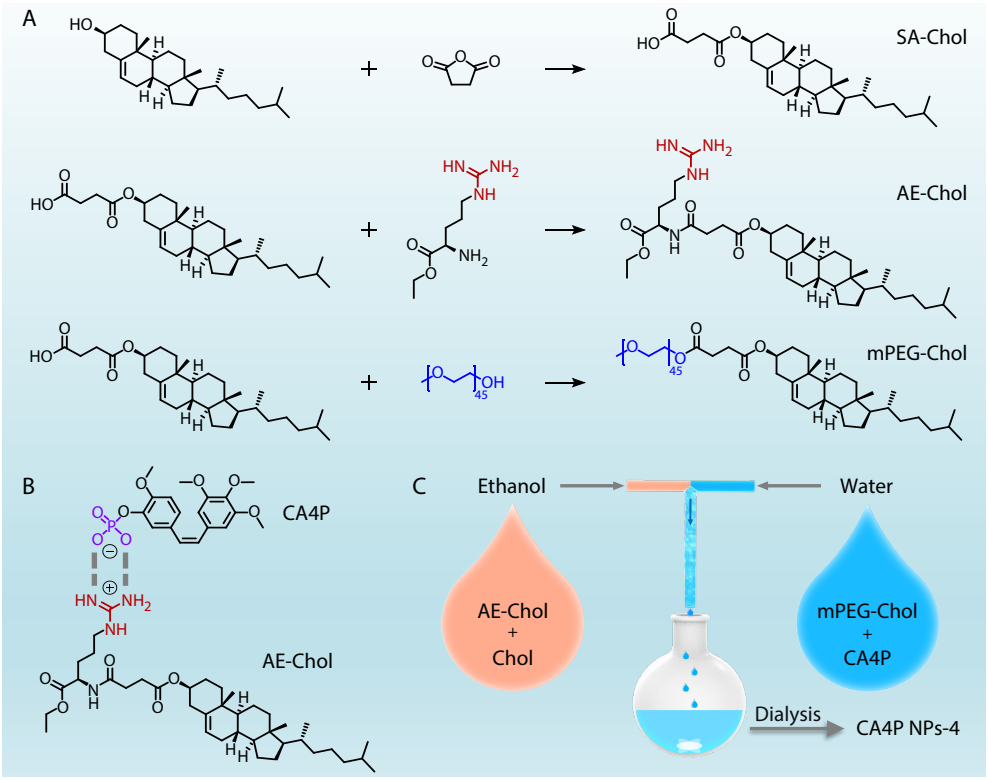

Fig. 1 Synthesis of various cholesterol derivatives and the preparation of CA4P NPs-4.

The CA4P NPs-4 were metabolized *in vivo* to arginine, cholesterol, ethanol and poly(ethylene glycol). Therefore, CA4P NPs-4 have high biological safety and show potential for clinical translation.

EXPERIMENTAL

Reagents

Cholesterol (Chol), H-Arg-OEt·2HCl (AE), succinic anhydride (SA) and dimethylaminopyridine (DMAP) were purchased from Shanghai Macklin Biochemical Co., Ltd. *N,N*-carbonyldiimidazole (CDI) and *N,N*-diisopropylethylamine (DIPEA) were purchased from Sun Chemical Technology Co., Ltd. Methoxypoly(ethylene glycol) (mPEG-OH, M_n=2.0×10^3 g/mol) was purchased from Jenkem Technology Co., Ltd. Combretastatin A4 phosphate (CA4P) was purchased from Shanghai Bide Pharmaceutical Technology Co., Ltd.

Instruments

^{1}H-NMR spectra were recorded on a Bruker AV 300 NMR (China) spectrometer in chloroform-d. Electron spray ionization mass spectrometry (ESI-MS) and matrix-assisted laser desorption/ionization mass spectrometry time of flight mass spectrometry (MALDI-TOF MS) were performed using a Thermo LTQ XL ion trap mass spectrometer. The zeta potentials and particle sizes were measured using Malvern Zetasizer Pro (United Kingdom). The ultraviolet/visible absorption (UV/Vis) spectra were measured using a UV-2401PC spectrophotometer (Japan). UV high-performance liquid chromatography (UV-HPLC) was performed using the Dalian Elite Analytical Instrument (China) and INano L microfluidic device (Micro&Nano Biologics Co., Ltd., China).

Cell Lines and Animals

The murine H22 hepatoma cell line was purchased from Shanghai Bogoo Biotechnology Co., Ltd., (China). Six to eight-weeks old female BALB/c mice (16–18 g) were purchased from Beijing Vital River Laboratory Animal Technology Co., Ltd., (China). All animal experiments were performed according to the Guidelines for Care and Use of Laboratory Animals of Jilin University, and approved by the Animal Ethics Committee of Jilin University.

Preparation of Cholesterol Derivatives

SA-Chol

Chol (1.0 equiv.), SA (1.5 equiv.) and DMAP (0.2 equiv.) were added to a round-bottomed flask, dissolved with anhydrous pyridine and reacted at 80 °C for 3 h. The pyridine was drained and then dissolved in anhydrous dichloromethane (DCM), and washed with 0.1 mol/L HCl. After recrystallization in *n*-hexane, the white solid SA-Chol was obtained (yield 95.5%) and characterized by ^{1}H-NMR and ESI-MS (ESI$^+$).

AE-Chol

SA-Chol (1.0 equiv.) and CDI (2.0 equiv.) were added to a round-bottomed flask and dissolved in anhydrous DCM, reacted overnight at 30 °C, and washed with brine to obtain Chol-CDI. Arg-EED·2HCl (1.0 equiv.) and DIPEA (1.0 equiv.) were dissolved in anhydrous *N,N*-dimethylformamide (DMF), and Chol-CDI (1.2 equiv.) was dissolved in anhydrous DCM and added to the mixture. The reaction was performed overnight at 45 °C. After precipitation and washing with ethyl ether for 3 times, the white solid AE-Chol was obtained (yield 63.2%) and characterized by

https://doi.org/10.1007/s10118-023-2921-7

^{1}H-NMR and ESI-MS (ESI$^+$).

mPEG-Chol

mPEG-OH (1.0 equiv.) was dissolved in anhydrous DMF and SA-Chol (1.5 equiv.), and DIC (1.5 equiv.) and DMAP (1.0 equiv.) were dissolved in anhydrous DCM. Both solutions were mixed and reacted at 35 °C for 48 h. The mixture was precipitated by ethyl ether, and the precipitate was redissolved in DMF and dialyzed against water for 48 h (MWCO=1.0 kDa). The white solid mPEG-Chol was obtained (yield 93.5%) after freeze-drying and characterized by ^{1}H-NMR and MALDI-TOF MS.

CA4P Loading by Film Hydration and Microfluidic

Film hydration

AE-Chol (1.0 equiv.), mPEG-Chol (1.0 equiv.) and Chol (0 or 1.0 equiv.) were added to a round-bottomed flask and dissolved in DCM. The solvent was removed by rotary evaporation, leaving a residual film. CA4P (1.0 equiv.) was dissolved in water and heated to 50 °C, and then added to the round-bottomed flask containing the carrier film and incubated at 50 °C for 1 h to obtain CA4P NPs-1 and CA4P NPs-3.

Microfluidics

AE-Chol and Chol were dissolved in ethanol, and mPEG-Chol and CA4P were dissolved in water. Both solutions were mixed by INano L and ultrafiltered by Millipore Amicon Ultra (MWCO=3.0 kDa) to obtain CA4P NPs-2 and CA4P NPs-4.

The drug loading efficiency (DLE) and the drug loading content (DLC) of the nanoparticles above are calculated according to the following formulas: DLE = the weight of loaded CA4P/the weight of feeding CA4P × 100%; DLC = the weight of loaded CA4P/the weight of CA4P nanoparticles × 100%.

Establishment of *In vivo* Tumor Model

The murine H22 tumor model was established by injecting BALB/c mice with H22 cells (3×10^5 cells per mouse) into their right abdomen. When the tumors reached approximately 100 mm^3, the mice were randomly divided into 3 groups (n=5) and respectively injected with PBS, CA4P (30 mg/kg) and CA4P NPs (30 mg/kg CA4P). The tumor sizes and body weight changes were recorded every other day. The tumor volume was calculated as follows: Tumor volume = 0.5 × length × width^2. The mice were sacrificed at the end of the treatment. The normal tissues and tumors were excised for routine H&E staining.

Statistical Analysis

Data are presented as the mean ± standard deviation (n=3) and compared by the Student's t-test. Statistical significances were set as follows: *p<0.05; highly significant: **p<0.01; ns: not significant.

RESULTS AND DISCUSSION

Characterization of SA-Chol, AE-Chol and mPEG-Chol

The ^{1}H-NMR spectrum of SA-Chol (Fig. 2A) shows peaks a and b of the methylene group at δ=2.61 ppm and δ=2.65 ppm, respectively, which are formed by the ring opening of

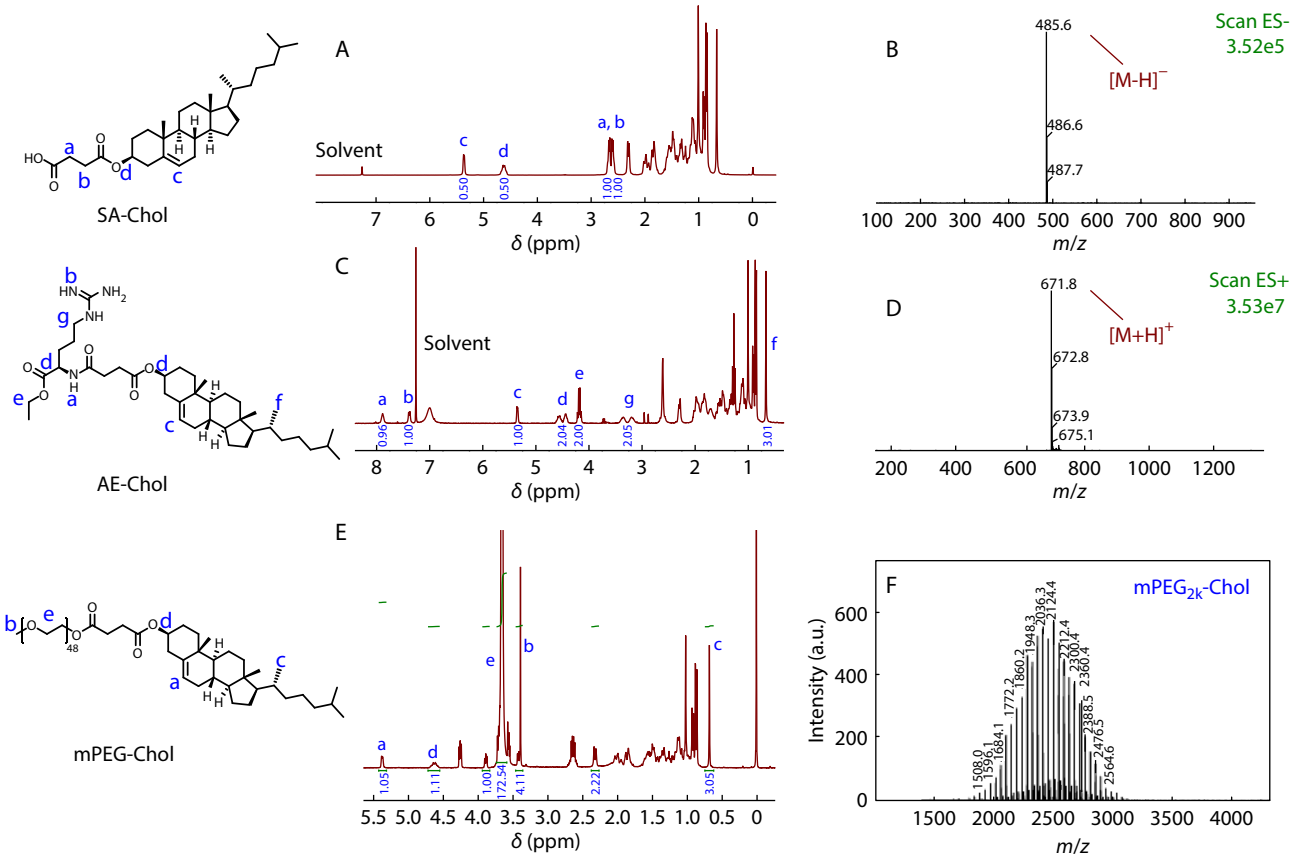

Fig. 2 The ^{1}H-NMR and ESI MS spectra of (A, B) SA-Chol, (C, D) AE-Chol, and the (E) ^{1}H-NMR and (F) MALDI-TOF MS spectra of mPEG-Chol.

https://doi.org/10.1007/s10118-023-2921-7

cholesterol-triggered succinic anhydride. The peaks c and d of the methyne group at δ=5.37 ppm and δ=4.64 ppm corresponded to cholesterol. The ratio of the peak a, peak b, peak c and peak d areas was 0.5:0.5:1:1, which indicated successful synthesis of SA-Chol. The ESI MS (*m/z*) for $C_{31}H_{50}O_4$ $[M-H]^-$ was 485.6 (Fig. 2B). In the ^{1}H-NMR spectrum of AE-Chol (Fig. 2C), the ratio of peak e (δ=4.17 ppm) to peak f (δ=0.67 ppm) area was 2:3, which indicated the successful acquisition of AE-Chol. The ESI MS (*m/z*) for $C_{39}H_{66}N_4O_5$ $[M+H]^+$ was 671.8 (Fig. 2D). In the ^{1}H-NMR of mPEG-Chol (Fig. 2E), the ratio of peak e (δ=3.64 ppm, $-CH_2-CH_2-$ of mPEG) to peak a (δ=5.37 ppm, —CH— of cholesterol) area was 172.5:1.0, which was indicative of the successful condensation of mPEG-OH with Chol into mPEG-Chol. As shown in Fig. 2(F), the MALDI-TOF MS (*m/z*) for mPEG-Chol was 2594.2, which is 469.8 (the molecular weight of the bonded cholesterol group) more than that of mPEG-OH (2124.4) and confirmed the successful synthesis of mPEG-Cho1 (Fig. S1 in the electronic supplementary information, ESI).

Characterization of CA4P NPs

As the guanidine$^+$/phosphate$^-$ salt bridge bound tightly in neutral and basic solution, four CA4P NPs were obtained through the salt-bridging interaction of the phosphate in CA4P with the guanidine group in AE-Chol by film hydration and microfluidic methods. The DLE by film hydration (CA4P NPs-1, Fig. 3A) and microfluidic (CA4P NPs-2, Fig. 3B) without the addition of Chol were 21.63% and 18.43%, the zeta potentials for both NPs were positive, and the particle size distributions were not uniform. Although the guanidine group coordinated with phosphate to form a hydrophobic core together with the hydrophobic Chol in mPEG-Chol, the results showed that the encapsulation of CA4P was ineffective, and the particle structure was not stable enough. Thus, Chol was added to form more stable nanoparticles. After addition of Chol, the DLEs increased with both film hydration (CA4P NPs-3, DLE=73.15%) and microfluidic (CA4P NPs-4, DLE=93.00%) methods (Fig. 3C). However, the zeta potential of CA4P NPs-3 was still positive and the particle size was not homogeneous. In contrast, the particle size of CA4P NPs-4 (Fig. 3D) obtained by microfluidic method was homogeneous, which was about 54.1 nm, and showed good stability in PBS buffer (Fig. S2 in ESI). Thus, the microfluidic method was the most effective way for synthesizing CA4P NPs, and the content of each component was optimized accordingly (Fig. S2 in ESI). After quantifying the CA4P absorption peak (wavelength=290 nm) by UV/Vis, AE-Chol, Chol, mPEG-Chol and CA4P added in the proportion of 1:0.5:1:1 resulted in 93% DLE and 10.5% DLC (Fig. 3E). Meanwhile, as we can see in Fig. 3(F), the CA4P NPs-4 achieved a sustained release of CA4P (12.2% at 2 h and 39.6% at 24 h), therefore, CA4P NPs-4 was used for the subsequent experiments.

In vivo Anti-tumor Efficacy

The mice in the PBS control group show rapid tumor growth, while both CA4P (30 mg/kg) and CA4P NPs-4 (30 mg/kg CA4P) inhibited the growth of H22 tumors in BALB/c mice (Figs. 4A and 4C). In fact, one mouse in the CA4P NPs-4 group develops tumor crusting and shedding (Fig. 4D) without causing any obvious change in body weight (Fig. 4B). While both CA4P and CA4P NPs-4 were safe at the dose of 30 mg/kg, CA4P NPs-4 inhibited tumor growth by 72.04% compared to the 24.64% inhibition rate achieved by CA4P.

Immunohistochemical Staining

To further assess the anti-tumor effects of the CA4P NPs, we analyzed the histopathological changes in the tumors and normal tissues. As shown in Fig. 5(A), the tumors in the PBS-

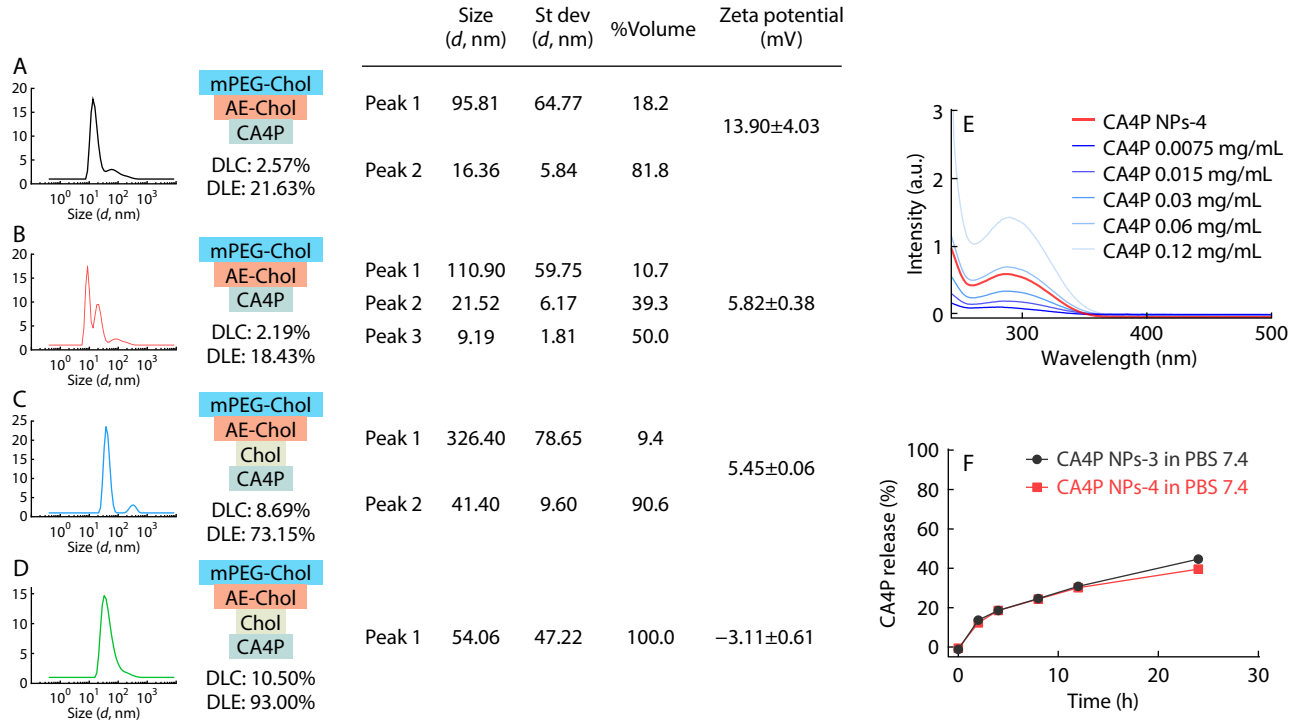

Fig. 3 The characterization of (A) CA4P NPs-1, (B) CA4P NPs-2, (C) CA4P NPs-3 and (D) CA4P NPs-4 *via* film hydration or microfluidic; (E) The DLC and DLE measurements of CA4P NPs-4; (F) The CA4P release of CA4P NPs-3 and CA4P NPs-4.

https://doi.org/10.1007/s10118-023-2921-7

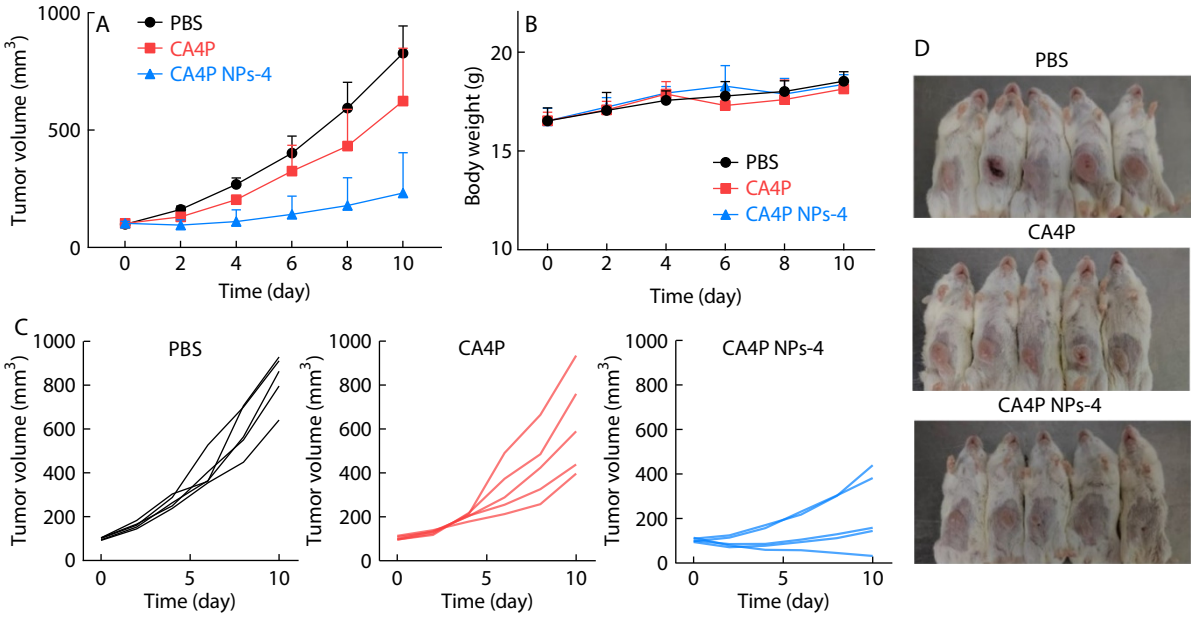

Fig. 4 (A) Tumor volume and (B) body weight changes during the treatment; (C) Tumor growth trend of each mouse; (D) Photos of the tumor bearing mice after various treatments. Results are presented as mean ± SD; *p<0.05, **p<0.01, ns: not significant.

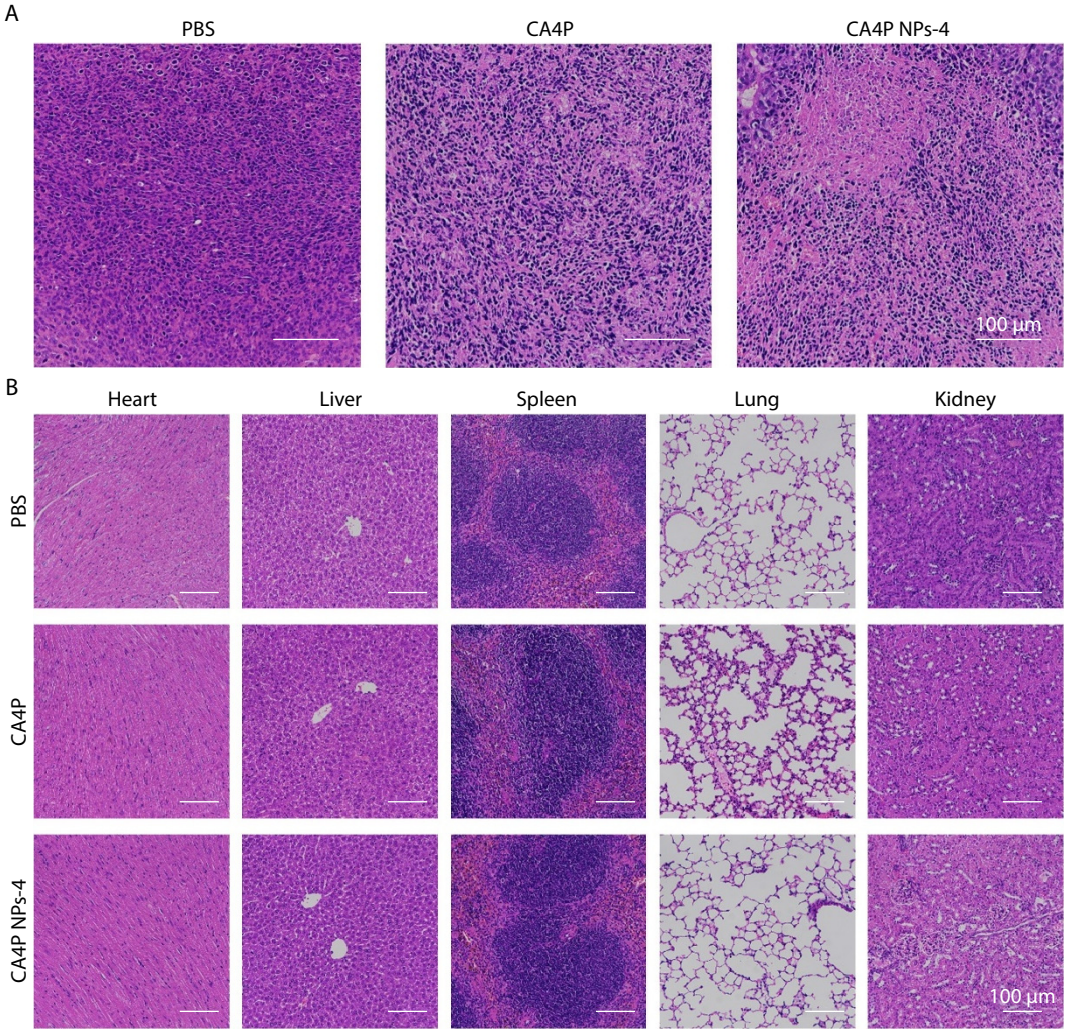

Fig. 5 H&E staining of (A) tumors or (B) normal tissues after various treatments.

https://doi.org/10.1007/s10118-023-2921-7

treated mice show rapidly proliferating cells, as indicated by distinct nuclei with abundant nucleoplasm and large nucleoli. Treatment with CA4P and CA4P NPs-4 significantly decreased tumor cell density, and partial necrotic areas can be observed in the CA4P group. No significant changes can be observed in normal tissues in any of the treatment groups (Fig. 5B), which further demonstrates that CA4P NPs-4 has excellent anti-tumor efficacy and biosafety.

CONCLUSIONS

We designed multi-component CA4P polymeric nanoparticles *via* the salt bridge of phosphate group and guanidine group. The CA4P NPs-4 synthesized by the microfluidic method had high drug loading efficacy and stability, and achieved sustained release of CA4P, with translated to significantly higher tumor inhibition rate compared to CA4P, demonstrates a high safety profile and strong clinical translation potential.

Conflict of Interests

The authors declare no interest conflict.

Electronic Supplementary Information

Electronic supplementary information (ESI) is available free of charge in the online version of this article at http://doi.org/10.1007/s10118-023-2921-7.

ACKNOWLEDGMENTS

This work was financially supported by the Ministry of Science and Technology of China (No. 2022YFE0110200), the Natural Science Foundation of Hunan Province of China (No. 2021JJ30680) and the National Natural Science Foundation of China (Nos. 52203198, 52025035 and 52103195).

REFERENCES

1 Askoxylakis, V.; Arvanitis, C. D.; Wong, C. S. F.; Ferraro, G. B.; Jain, R. K. Emerging strategies for delivering antiangiogenic therapies to primary and metastatic brain tumors. *Adv. Drug Deliv. Rev.* **2017**, *119*, 159–174.
2 Li, Z.; Di, C.; Li, S.; Yang, X.; Nie, G. Smart nanotherapeutic targeting of tumor vasculature. *Acc. Chem. Res.* **2019**, *52*, 2703–2712.
3 Yamakawa, D.; Kidoya, H.; Sakimoto, S.; Jia, W.; Takakura, N. 2-Methoxycinnamaldehyde inhibits tumor angiogenesis by suppressing Tie2 activation. *Biochem. Biophys. Res. Commun.* **2011**, *415*, 174–80.
4 Hong, S.; Zheng, D. W.; Zhang, C.; Huang, Q. X.; Cheng, S. X.; Zhang, X. Z. Vascular disrupting agent induced aggregation of gold nanoparticles for photothermally enhanced tumor vascular disruption. *Sci. Adv.* **2020**, *6*, eabb0020.
5 Smolarczyk, R.; Czapla, J.; Jarosz-Biej, M.; Czerwinski, K.; Cichon, T. Vascular disrupting agents in cancer therapy. *Eur. J. Pharmacol.* **2021**, *891*, 173692.
6 Daei Farshchi Adli, A.; Jahanban-Esfahlan, R.; Seidi, K.; Samandari-Rad, S.; Zarghami, N. An overview on Vadimezan (DMXAA): the vascular disrupting agent. *Chem. Biol. Drug Design* **2018**, *91*, 996–1006.
7 Liu, Z.; Yu, H.; Shen, N.; Tang, Z.; Chen, X. A ROS-stimulus-responsive nanocarrier loading with guanidine-modified hydroxycamptothecin prodrug for enhanced anti-tumor efficacy. *CCS Chem.* **2020**, *2*, 305–316.
8 Liu, Z. L.; Ma, S.; Sun, J. L.; Si, X. H.; Tang, Z. H.; Chen, X. S. Reactive oxygen species responsive core-shell nanoparticles increase tumor enrichment and endocytosis. *Acta Polymerica Sinica* (in Chinese) **2020**, *51*, 1153–1159.
9 Liu, Z.; Tang, Z.; Zhang, D.; Wu, J.; Si, X.; Shen, N.; Chen, X. A novel GSH responsive poly(alpha-lipoic acid) nanocarrier bonding with the honokiol-DMXAA conjugate for combination therapy. *Sci. China Mater.* **2019**, *63*, 307–315.
10 Dong, S.; Ma, S.; Liu, Z. L.; Ma, L. L.; Zhang, Y.; Tang, Z. H.; Deng, M. X.; Song, W. T. Functional amphiphilic poly(2-oxazoline) block copolymers as drug carriers: the relationship between structure and drug loading capacity. *Chinese J. Polym. Sci.* **2021**, *39*, 865–873.
11 Wang, T.; Wu, C.; Wang, C.; Zhang, G.; Arnst, K. E.; Yao, Y.; Zhang, Z.; Wang, Y.; Pu, D.; Li, W. Unraveling the molecular mechanism of BNC105, a phase II clinical trial vascular disrupting agent, provides insights into drug design. *Biochem. Biophys. Res. Commun* **2020**.
12 Liu, Z.; Zhang, Y.; Shen, N.; Sun, J.; Tang, Z.; Chen, X. Destruction of tumor vasculature by vascular disrupting agents in overcoming the limitation of EPR effect. *Adv. Drug Deliv. Rev.* **2022**, *183*, 114138.
13 Sherbet, G. V. Suppression of angiogenesis and tumour progression by combretastatin and derivatives. *Cancer Lett.* **2017**, *403*, 289–295.
14 Galbraith, S. M.; Chaplin, D. J.; Lee, F.; Stratford, M. R. L.; Locke, R. J.; Vojnovic, B.; Tozer, G. M. Effects of combretastatin A4 phosphate on endothelial cell morphology *in vitro* and relationship to tumour vascular targeting activity *in vivo*. *Anticancer Res.* **2001**, *21*, 93–102.
15 Hasani, A.; Leighl, N. Classification and toxicities of vascular disrupting agents. *Clinical Lung Cancer* **2011**, *12*, 18–25.
16 Dong, M.; Liu, F.; Zhou, H.; Zhai, S.; Yan, B. Novel Natural product- and privileged scaffold-based tubulin inhibitors targeting the colchicine binding site. *Molecules* **2016**, *21*, 1375.
17 An, Y.; Chen, C.; Zhu, J. D.; Dwivedi, P.; Zhao, Y. J.; Wang, Z. Hypoxia-induced activity loss of a photo-responsive microtubule inhibitor azobenzene combretastatin A4. *Front. Chem. Sci. Eng.* **2020**, *14*, 880–888.
18 Winn, B. A.; Devkota, L.; Kuch, B.; MacDonough, M. T.; Strecker, T. E.; Wang, Y.; Shi, Z.; Gerberich, J. L.; Mondal, D.; Ramirez, A. J.; Hamel, E.; Chaplin, D. J.; Davis, P.; Mason, R. P.; Trawick, M. L.; Pinney, K. G. Bioreductively activatable prodrug conjugates of combretastatin A-1 and combretastatin A-4 as anticancer agents targeted toward tumor-associated hypoxia. *J. Nat. Prod.* **2020**, *83*, 937–954.
19 Welford, A. F.; Biziato, D.; Coffelt, S. B.; Nucera, S.; Fisher, M.; Pucci, F.; Di Serio, C.; Naldini, L.; De Palma, M.; Tozer, G. M.; Lewis, C. E. TIE2-expressing macrophages limit the therapeutic efficacy of the vascular-disrupting agent combretastatin A4 phosphate in mice. *J. Clin. Invest.* **2011**, *121*, 1969–73.
20 Jaroch, K.; Karolak, M.; Gorski, P.; Jaroch, A.; Krajewski, A.; Ilnicka, A.; Sloderbach, A.; Stefanski, T.; Sobiak, S. Combretastatins: *in vitro* structure-activity relationship, mode of action and current clinical status. *Pharmacol. Rep.* **2016**, *68*, 1266–1275.
21 Liu, Y.; Wang, S.; Zhao, X.; Feng, Y.; Bormans, G.; Swinnen, J.; Oyen, R.; Huang, G.; Ni, Y.; Li, Y. Predicting clinical efficacy of vascular disrupting agents in rodent models of primary and secondary liver cancers: an overview with imaging-histopathology correlation. *Diagnostics* **2020**, *10*, 78.

22 Hinnen, P.; Eskens, F. A. Vascular disrupting agents in clinical development. *Br. J. Cancer* **2007**, *96*, 1159–1165.
23 Gao, M.; Zhang, D.; Yao, N.; Jin, Q.; Jiang, C.; Zhang, J.; Wang, F. Enhancing intratumoral biodistribution and antitumor activity of nab-paclitaxel through combination with a vascular disrupting agent, combretastatin A-4-phosphate. *Cancer Chemoth. Pharmacol.* **2019**, *84*, 1187–1194.
24 Brown, A. W.; Holmes, T.; Fisher, M.; Tozer, G. M.; Harrity, J. P. A.; Kanthou, C. Evaluation of sydnone-based analogues of combretastatin A-4 phosphate (CA4P) as vascular disrupting agents for use in cancer therapy. *Chem. Med. Chem.* **2018**, *13*, 2618–2626.
25 Liu, T. Z.; Zhang, D. W.; Song, W. T.; Tang, Z. H.; Zhu, J. M.; Ma, Z. M.; Wang, X. D.; Chen, X. S.; Tong, T. A poly(L-glutamic acid)-combretastatin A4 conjugate for solid tumor therapy: Markedly improved therapeutic efficiency through its low tissue penetration in solid tumor. *Acta Biomaterialia* **2017**, *53*, 179–189.
26 Folkman, J. Role of angiogenesis in tumor growth and metastasis. *Semin. Oncol.* **2002**, *29*, 15–8.
27 Liu, Z. L.; Shen, N.; Tang, Z. H.; Zhang, D. W.; Ma, L. L.; Yang, C. G.; Chen, X. S. An eximious and affordable GSH stimulus-responsive poly(alpha-lipoic acid) nanocarrier bonding combretastatin A4 for tumor therapy. *Biomater. Sci-Uk.* **2019**, *7*, 2803–2811.
28 Deng, C.; Zhao, J.; Zhou, S.; Dong, J.; Cao, J.; Gao, J.; Bai, Y.; Deng, H. The vascular disrupting agent CA4P improves the antitumor efficacy of CAR-T cells in preclinical models of solid human tumors. *Mol. Ther.* **2020**, *28*, 75–88.
29 Thebault, C. J.; Ramniceanu, G.; Boumati, S.; Michel, A.; Seguin, J.; Larrat, B.; Mignet, N.; Menager, C.; Doan, B. T. Theranostic MRI liposomes for magnetic targeting and ultrasound triggered release of the antivascular CA4P. *J. Control. Rel.: Official J. Control. Rel. Soc.* **2020**, *322*, 137–148.
30 Satterlee, A. B.; Rojas, J. D.; Dayton, P. A.; Huang, L. Enhancing nanoparticle accumulation and retention in desmoplastic tumors *via* vascular disruption for internal radiation therapy. *Theranostics* **2017**, *7*, 253–269.

https://doi.org/10.1007/s10118-023-2921-7